Biochimica et Biophysica Acta 1812 (2011) 59–69

Contents lists available at ScienceDirect

Biochimica et Biophysica Acta

journal homepage: www.elsevier.com/locate/bbadis

Mutations in cytoplasmic dynein lead to a Huntington's disease-like defect in energy metabolism of brown and white adipose tissues

Judith Eschbach [a,b], Anissa Fergani [a,b], Hugues Oudart [c], Jean-Patrice Robin [c], Frédérique Rene [a,b], Jose-Luis Gonzalez de Aguilar [a,b], Yves Larmet [a,b], Joffrey Zoll [d,e], Majid Hafezparast [f], Birgit Schwalenstocker [g], Jean-Philippe Loeffler [a,b], Albert C. Ludolph [g], Luc Dupuis [a,b,*]

[a] Inserm, U692, Strasbourg, F-67085 France
[b] Université de Strasbourg, Faculté de Médecine, UMRS692, Strasbourg, F-67085 France
[c] DEPE, IPHC, Strasbourg, France
[d] Université de Strasbourg, Faculté de Médecine, Physiology Department, Université de Strasbourg, EA 3072, Strasbourg, France
[e] CHRU of Strasbourg, Physiology and Functional Explorations Department, New Civil Hospital, B.P. 426, 67091 Strasbourg, France
[f] University of Sussex, Brighton, BN1 9QG, UK
[g] Department of Neurology, University of Ulm, Ulm, Germany

ARTICLE INFO

Article history:
Received 18 June 2010
Received in revised form 8 September 2010
Accepted 22 September 2010
Available online 29 September 2010

Keywords:
White adipose tissue
Brown adipose tissue
Thermogenesis
Lipolysis
Huntington's disease
Molecular motors
Lipid droplets

ABSTRACT

The molecular motor dynein is regulated by the huntingtin protein, and Huntington's disease (HD) mutations of huntingtin disrupt dynein motor activity. Besides abnormalities in the central nervous system, HD animal models develop prominent peripheral pathology, with defective brown tissue thermogenesis and dysfunctional white adipocytes, but whether this peripheral phenotype is recapitulated by dynein dysfunction is unknown. Here, we observed prominently increased adiposity in mice harboring the *legs at odd angles* (*Loa*/+) or the *Cramping* mutations (*Cra*/+) in the dynein heavy chain gene. In *Cra*/+ mice, hyperadiposity occurred in the absence of energy imbalance and was the result of impaired norepinephrine-stimulated lipolysis. A similar phenotype was observed in 3T3L1 adipocytes upon chemical inhibition of dynein showing that loss of functional dynein leads to impairment of lipolysis. *Ex vivo*, dynein mutant adipose tissue displayed increased reactive oxygen species production that was, at least partially, responsible for the decreased cellular responses to norepinephrine and subsequent defect in stimulated lipolysis. Dynein mutation also affected norepinephrine efficacy to elicit a thermogenic response and led to morphological abnormalities in brown adipose tissue and cold intolerance in dynein mutant mice. Interestingly, protein levels of huntingtin were decreased in dynein mutant adipose tissue. Collectively, our results provide genetic evidence that dynein plays a key role in lipid metabolism and thermogenesis through a modulation of oxidative stress elicited by norepinephrine. This peripheral phenotype of dynein mutant mice is similar to that observed in various animal models of HD, lending further support for a functional link between huntingtin and dynein.

1. Introduction

The cell cytoskeleton is a network of different types of filaments on which molecular motors drive specific cargoes. Microtubules constitute one of the major cytoskeletal filaments and two types of motors, namely, cytoplasmic dynein (later referred as dynein) and kinesins, use them as railroad tracks. Dynein is the only motor that drives cargoes towards the minus end of microtubules and, as such, appears responsible for most, if not all, the transport of cargoes from the cell periphery towards the cell body. Dynein is involved in the late phases of mitosis, and its function has been extensively studied in neurons in which it appears crucial for retrograde transport in axons [1] and dendritic morphogenesis [2].

Studies on dynein functions have been previously hampered by the lack of genetic tools. Indeed, the complexity of the motor, with numerous subunits yielding a 2-million-Da molecular complex, renders gain-of-function experiments currently impossible. Conversely, embryos with ablated dynein heavy chain do not survive, showing the important functions of dynein during development [3]. However, mice with mildly compromised dynein function have been generated in 2003 by Hafezparast and collaborators [4]. These authors showed that two independent mouse strains generated by *N*-ethyl-*N*-nitrosourea-induced mutagenesis, *Legs at odd angles* (*Loa*) and *Cramping 1* (*Cra1*, further referred to as *Cra*), harbored dominantly inherited missense point mutations in the cargo-binding domain of the dynein heavy chain 1. The *Loa* and *Cra* mutations did not appear to affect basic cellular functions of

* Corresponding author. INSERM U692, Faculté de Médecine, bat 3, 8e étage, 11 rue Humann, Strasbourg, F-67085, France. Tel.: +33 3 68 85 30 91; fax: +33 3 68 85 30 65.
E-mail address: ldupuis@unistra.fr (L. Dupuis).

0925-4439/$ – see front matter © 2010 Elsevier B.V. All rights reserved.
doi:10.1016/j.bbadis.2010.09.009

dynein such as mitosis. However, dynein mutation impaired the ability of dynein motors to sustain fast retrograde transport leading to a decreased efficiency of these motors in situations of cellular stress [4,5] and retrograde transport in adult *Loa*/+ motor neurons was decreased [4,5]. Homozygous mice die at birth, but heterozygous mice are viable and present with a striking motor phenotype later ascribed to an early-onset proprioceptive sensory neuropathy [6–8].

Dynein dysfunction is a potential causal mechanism in neurodegenerative diseases, most notably in degenerative diseases of the striatum such as Huntington's disease (HD). Indeed, huntingtin, the protein mutant in HD, and its associated protein HAP1 are binding partners of dynein, and the activity of the dynein motor is positively regulated by wild-type huntingtin and strongly decreased by HD-associated mutations of huntingtin [9,10]. Our most recent studies showed that *Cra*/+ mice developed striatal atrophy and its expected behavioral and pathological consequences [11]. These results show that a point mutation in dynein is sufficient to lead to a pathology analogous to HD, although milder.

Besides central nervous system pathology, it is increasingly recognized that HD leads to a number of peripheral defects. Indeed, HD-associated mutations of huntingtin have systemic effects on energy metabolism. In particular, HD animal models develop defects in both brown and white adipose tissues leading to compromised lipolysis and thermogenesis [12–14]. Whether dynein dysfunction leads to similar defects in the periphery remains unknown. We studied here the peripheral phenotype of dynein mutant mice and showed that dynein mutations compromise adipose tissue lipolysis and thermogenesis. We further provide evidence that the defect triggered by mutant dynein is due, at least in part, to increased oxidative stress in response to norepinephrine. Interestingly, protein levels of huntingtin were decreased in dynein mutant adipose tissue. This peripheral phenotype of dynein mutant mice is similar to that observed in various animal models of HD, lending further support for a functional link between huntingtin and dynein.

2. Materials and methods

2.1. Animals

All the experiments were performed on male mice. Heterozygous *Cra*/+ mice were F1 generation of a C57Bl6/C3H crossing and were identified by tail DNA genotyping as described previously [4]. Wild-type littermates were used as controls. Heterozygous *Loa*/+ mice were in a pure C57Bl6 background. Mice were maintained at 23 °C with a 12-h light/dark cycle and had food and water *ad libitum*. For biochemical analysis, animals were sacrificed at the ages indicated in the figures (2, 4, and 8 months of age), and tissues were quickly dissected, frozen in liquid nitrogen, and stored at −80 °C until use. All animal experiments were performed under the supervision of authorized investigators and followed current EU regulations. For the high-fat diet (HFD) experiments, C57Bl6/C3H wild-type mice were fed with chow diet supplemented with 20% (wt/wt) saturated fat.

2.2. RT-qPCR

Real-time RT quantitative PCR was performed as described [7]. The relative levels of each RNA were normalized to the corresponding polymerase II RNA levels. Table S1 indicates the primers used for qPCR.

2.3. Histology

For adipose tissues histology, 24-h post-fixed tissues were embedded in paraffin and cut on a microtome into slices of 16-μm thickness. Sections were then deparaffinized and rehydrated before hematoxylin and eosin staining and then dehydrated for observation.

2.4. Leptin ELISA

Leptin levels in serum were measured using an ELISA kit from Assay Pro (St. Charles, MO, USA), following instructions of the manufacturer.

2.5. Indirect calorimetry

We measured O_2 consumption and CO_2 production by using an open-circuit indirect calorimetry system (Klogor, Lannion, France) as described [15]. Energy expenditure was calculated during a 24-h cold challenge at 7 °C.

2.6. Body composition analysis

Carcasses were freeze-dried to constant mass and ground under liquid nitrogen to a fine homogenous powder kept at −20 °C until chemical analysis. Samples were lyophilized for 48 h just before analysis to eliminate any traces of water. Body lipid content was determined on duplicate samples by a solvent extraction procedure (chloroform/methanol; 2/1, v/v) adapted from Folch et al. [16] on 1 g of powder. The nitrogen content of the carcass was determined in triplicate using the Kjeldahl method on 100–150 mg of sample. Protein content was calculated as nitrogen content *6.25. Ash content was measured on duplicate 1- to 2-g samples after total combustion at 400 °C for 24 h in a muffle furnace.

2.7. Western blot

White adipose tissue (WAT) pads were lysed and homogenized in a protein extraction buffer (PBS 1×, 0.1% SDS, 0.2% IGEPAL, 1% deoxycholate, 1× protease inhibitor cocktail, and 1× phosphatase inhibitor) using a Potter homogenizer (VWR, Strasbourg, France). Protein quantification was carried out using a BCA assay kit (Interchim, Montlucon, France). Equal amounts of soluble proteins were denaturated by boiling, resolved by sodium dodecyl sulfatepolyacrylamide gel electrophoresis (SDS-PAGE) and transferred to a nitrocellulose membrane. After blocking in 10% non-fat dry milk in wash buffer for 30 min, and probing with a specific primary antibody targeted at hormone-sensitive lipase (HSL), HSL phosphorylated at Serine 563 (P-HSL(Ser-563)), adipose triglyceride lipase (ATGL), and a phosphorylated form of a PKA substrate (PKA-S) (all from Cell Signaling, Boston, MA) and actin (Sigma-Aldrich, Lyon, France) and a horseradish peroxidase (HRP)-conjugated secondary antibody (Jackson Immunoresearch, Suffolk, United Kingdom), the protein bands were detected by chemiluminescence and X-ray film exposure (GE healthcare, Chalfont St. Giles, United Kingdom). Results were quantified using imageJ software [17].

2.8. WAT explants and lipolysis assays

Epididymal WAT was dissected immediately after sacrifice, weighed, and minced with scissors in warm glucose-free Krebs–Ringer bicarbonate buffer, pH 7.4 containing 4% BSA. Samples were incubated in 3 ml of buffer, pretreated or not with 1 mM EHNA (erytro-9-(2-Hydroxy-3-nonyl) adenine hydrochloride, Sigma-Aldrich, Lyon France) or 10 μM apocynin for 15 min, and then stimulated with 10 μM isoproterenol or 10 μM forskolin. Incubation medium was collected and assayed for glycerol content (Randox, Antrim, United Kingdom). Glycerol levels were normalized to the corresponding tissue weight. Similar results were obtained by standardization with protein content (not shown).

2.9. Cell culture and treatments

3 T3-L1 pre-adipocytes from ATCC (Manassas, USA) were grown until confluence in DMEM high glucose containing 10% FCS and 1% penicillin/streptomycin in plates coated with 0.01% collagen. After 2 days of confluence, cells were differentiated into adipocytes by

using DMEM high glucose containing 10% FCS, 1% penicillin/streptomycin, 1 μM dexamethasone (Sigma-Aldrich, Lyon, France), 0.5 mM of IBMX (3-isobutyl-1-methylxanthine, PDE inhibitor) (Sigma-Aldrich, Lyon France), and 1 μM insulin (Sigma-Aldrich, Lyon France) during 2 days. Cells were further maintained for 6 days in DMEM high glucose containing 10% FCS, 1 μM insulin, and 1% penicillin/streptomycin before experiments.

For lipolysis experiments, 4 h starved differentiated 3T3-L1 were pretreated with 1 mM EHNA for 15 min and stimulated with 10 μM isoproterenol (Sigma-Aldrich, Lyon, France) in the presence of 0.5 mM IBMX for 4 h. Lipid droplets were stained with bodipy 493/503 (Invitrogen, Cergy-Pontoise, France) and nuclei with Hoechst. Lipid droplets were visualized using epifluorescence microscopy. For quantification of the diameter of lipid droplets, we measured the area of the five largest lipid droplets per cell by using ImageJ software. This cutoff of 5 droplets per cell was chosen because (i) all cells studied showed at least 5 droplets and (ii) it was not possible to measure the diameter of most small droplets in conditions treated with isoproterenol (see Fig. 4B).

2.10. Oxidative stress measurements

WAT explants were incubated with 5 μM hydroethidine during 15 min and further stimulated with 10 μM isoproterenol. Tissues were immediately fixed in 4% PFA and mounted for observation. H_2O_2 production was measured with Amplex Red reagent (Invitrogen,

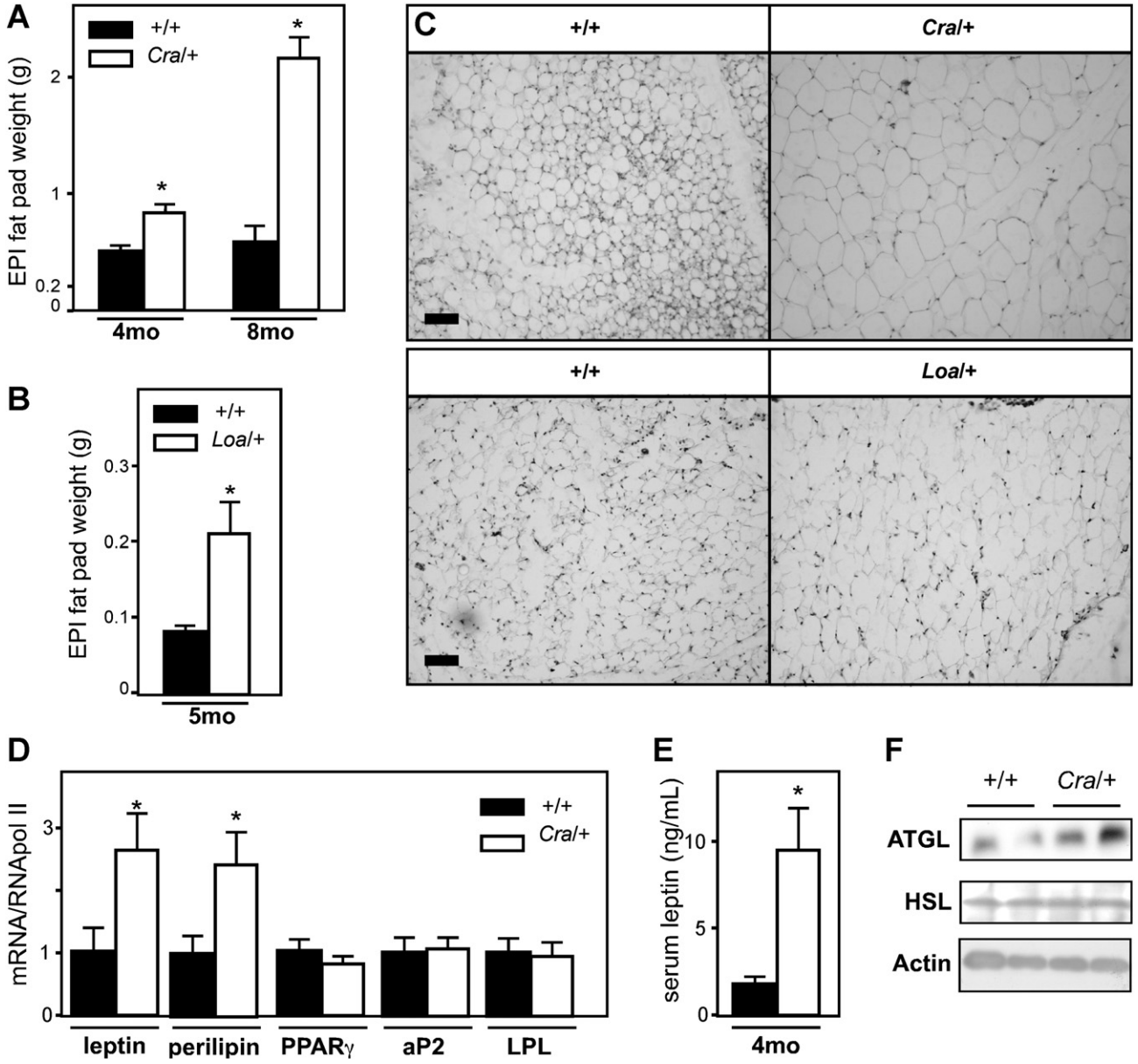

Fig. 1. Increased adiposity in dynein mutant mice. All values are indicated as mean ± SEM. Wild-type mice (+/+) are indicated using black symbols and dynein mutant mice (*Cra*/+ or *Loa*/+) using open symbols. (A) Epididymal white adipose tissue (WAT) fat pad weight in grams of +/+ and *Cra*/+ mice of 4 (4mo) and 8 (8mo) months of age. $N = 8$ per group. $^*p<0.05$ vs. corresponding +/+ in Student's *t*-test. (B) Epididymal WAT fat pad weight in g of +/+ and *Loa*/+ mice of 5 (5mo) months of age. $N = 7$ per group. $^*p<0.05$ vs. corresponding +/+ in Student's *t*-test. (C) Representative photomicrograph showing WAT sections of 8-month-old *Cra*/+ (upper panels) and 5-month-old *Loa*/+ (lower panels) mice and their corresponding +/+ mice stained with hematoxylin and eosin. Note the strong increase in adipocyte size. Scale bar = 25 μm. (D) mRNA levels of leptin, perilipin, peroxisome proliferation activating receptor γ (PPARγ), adipocyte protein 2 (aP2), and lipoprotein lipase (LPL) in the epididymal WAT from +/+ and *Cra*/+ mice at 4 months of age. $^*p<0.05$ vs. +/+ ($n = 5$–8 mice per group). (E) Leptin levels in serum from +/+ and *Cra*/+ mice at 4 months of age. $^*p<0.05$ vs. +/+ ($n = 4$–8 mice per group). (F) Representative Western blotting of adipose triglyceride lipase (ATGL), hormone-sensitive lipase (HSL), and actin in the epididimary WAT from 4-month-old +/+ and *Cra*/+ mice.

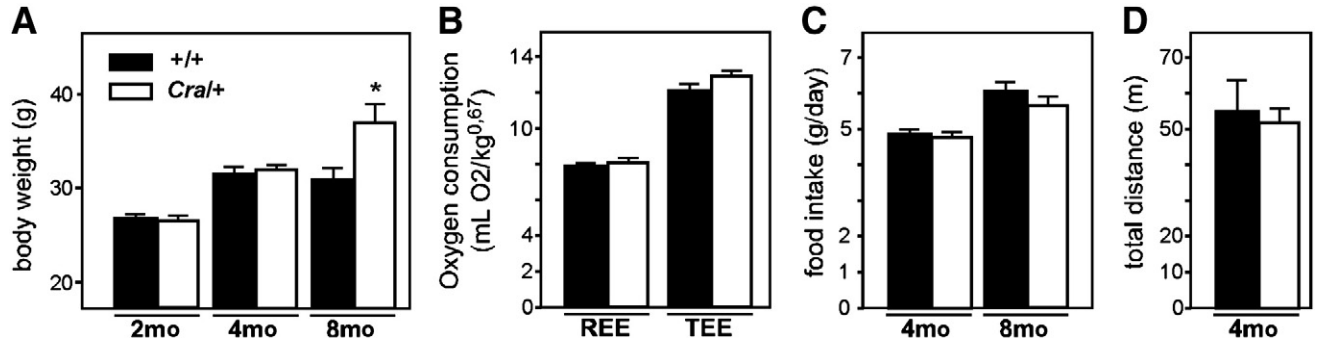

Fig. 2. Normal energy balance in dynein mutant mice. (A) Body weight of wild-type (+/+, black columns) and dynein mutant (*Cra*/+) mice at 2 (2mo), 4 (4mo), and 8 (8mo) months of age. $^{*}p<0.05$ vs. +/+ ($n=5$–8 mice per group). (B) Resting (REE) and total (TEE) energy expenditure of wild-type (+/+, black columns) and dynein mutant (*Cra*/+) mice at 4 months of age. There is no global decrease in energy expenditure in dynein mutant mice at this age. No significant difference is observed. $N=6$ per group. (C) Food intake of wild-type (+/+, black columns) and dynein mutant (*Cra*/+) mice at 4 (4mo) and 8 (8mo) months of age. No significant difference is observed. $N=10$ per group (D) Overnight spontaneous locomotor activity as measured using infrared beams in wild-type (+/+, black columns) and dynein mutant (*Cra*/+) mice at 4 (4mo) months of age. No difference is observed between both genotypes. $N=12$ per group.

Table 1
Body composition of dynein mutant mice.

	+/+, 4 Months ($n=9$)	*Cra*/+, 4 Months ($n=9$)
Body weight, g	28.7 ± 1.0	30.3 ± 1.2
Water, %	61.9 ± 1.3	59.9 ± 1.2
Proteins, g	5.66 ± 0.14	5.92 ± 0.15
Proteins, %	19.8 ± 0.5	19.6 ± 0.5
Lipids, g	4.24 ± 0.65	5.55 ± 0.83
Lipids, %	14.5 ± 1.7	17.8 ± 1.8
Minerals, g	1.13 ± 0.03	1.12 ± 0.03

Cergy-Pontoise, France), which reacts with H_2O_2 in a 1:1 stoichiometry catalyzed by HRP (Fluka Biochemika, Lyon, France) to yield the fluorescent compound resorufin and molar equivalent O_2. Resorufin has excitation/emission characteristics of 563/587 nm and is extremely stable once formed. Fluorescence was measured continuously [change in fluorescence (ΔF)/s] with a Fluoromax 4 (Jobin Yvon, Longjumeau, France) spectrofluorometer with temperature control and magnetic stirring. After baseline, ΔF (reactants only) was established, the reaction was initiated by addition of a weighed amount of minced WAT to 600 µl of *buffer Z* containing (in mM) 110 K-MES, 35 KCl, 1 EGTA, 10 K_2HPO_4, and 3 $MgCl_2$ (pH 7.3 at 37 °C). We first added 5 µM Amplex Red and 0.5 U/ml HRP. We recorded baseline production of H_2O_2 in these conditions and then added 10 µM isoproterenol to stimulate lipolysis. After 3 min of recordings, we added 10 µM apocynin and further recorded fluorescence for 3 min. H_2O_2 production rate was calculated from the slope of ΔF/s, after subtracting background, from a standard curve established with the

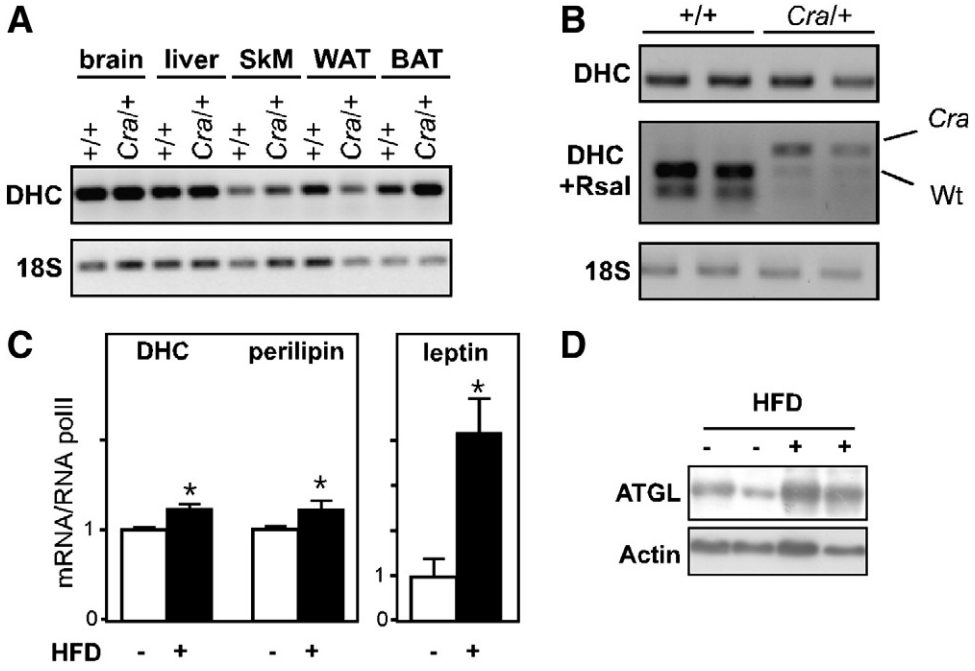

Fig. 3. Dynein is expressed in the WAT and regulated by high-fat feeding. (A) RT-PCR analysis of dynein heavy chain (DHC) and 18S ribosomal RNA in various tissues of +/+ and *Cra*/+ mice of 4 months of age. Note the broad expression pattern of dynein outside the CNS. (B) RT-PCR analysis of dynein heavy chain (DHC) and 18S ribosomal RNA in the WAT of +/+ and *Cra*/+ mice. The primers used for DHC cDNA amplification span the *Cra* mutation, and this mutation deletes an endogenous *Rsa*I site. Thus, digestion of the amplified DHC PCR product with *Rsa*I (middle panel, DHC + *Rsa*I) allows distinguishing between *Rsa*I-resistant *Cra* mutation bearing cDNAs and *Rsa*I-sensitive wild-type cDNAs. Two representative mice of each genotype are shown ($n=8$). The results indicate that both DHC alleles (wild type and *Cra*) are expressed in the WAT. (C) mRNA levels of dynein heavy chain (DHC), leptin and perilipin in the epididimary white adipose tissue from wild-type mice fed with chow (−) or high-fat diet (HFD, +). $^{*}p<0.05$ vs. chow. $n=6$ mice per group. (D) Representative Western blotting of ATGL and actin in the epididimary white adipose tissue from wild-type mice fed with chow (−) or high-fat diet (HFD, +).

appropriate reaction conditions. H_2O_2 production was expressed as picomoles per minute per milligram of wet weight.

2.11. Statistical analysis

Statistical comparisons were accomplished with the unpaired Student's *t*-test for comparison of two groups or ANOVA followed by the post hoc Newman–Keuls multiple comparisons test for multiple comparisons using PRISM version 2.0a software (GraphPad, San Diego, USA).

3. Results

3.1. Hyperadiposity in the absence of energy imbalance in dynein mutant mice

To explore the potential role of dynein in adipocytes, we used mice heterozygous for the Cramping mutation (*Cra*/+) and the Legs at odd angles mutation (*Loa*/+). Both *Loa*/+ and *Cra*/+ mice showed increased weight of the white adipose tissue (WAT), including epididymal (Fig. 1A and B), interscapular and retroperitoneal (data not shown) fat pads. Interestingly, increased mass of the fat pads was

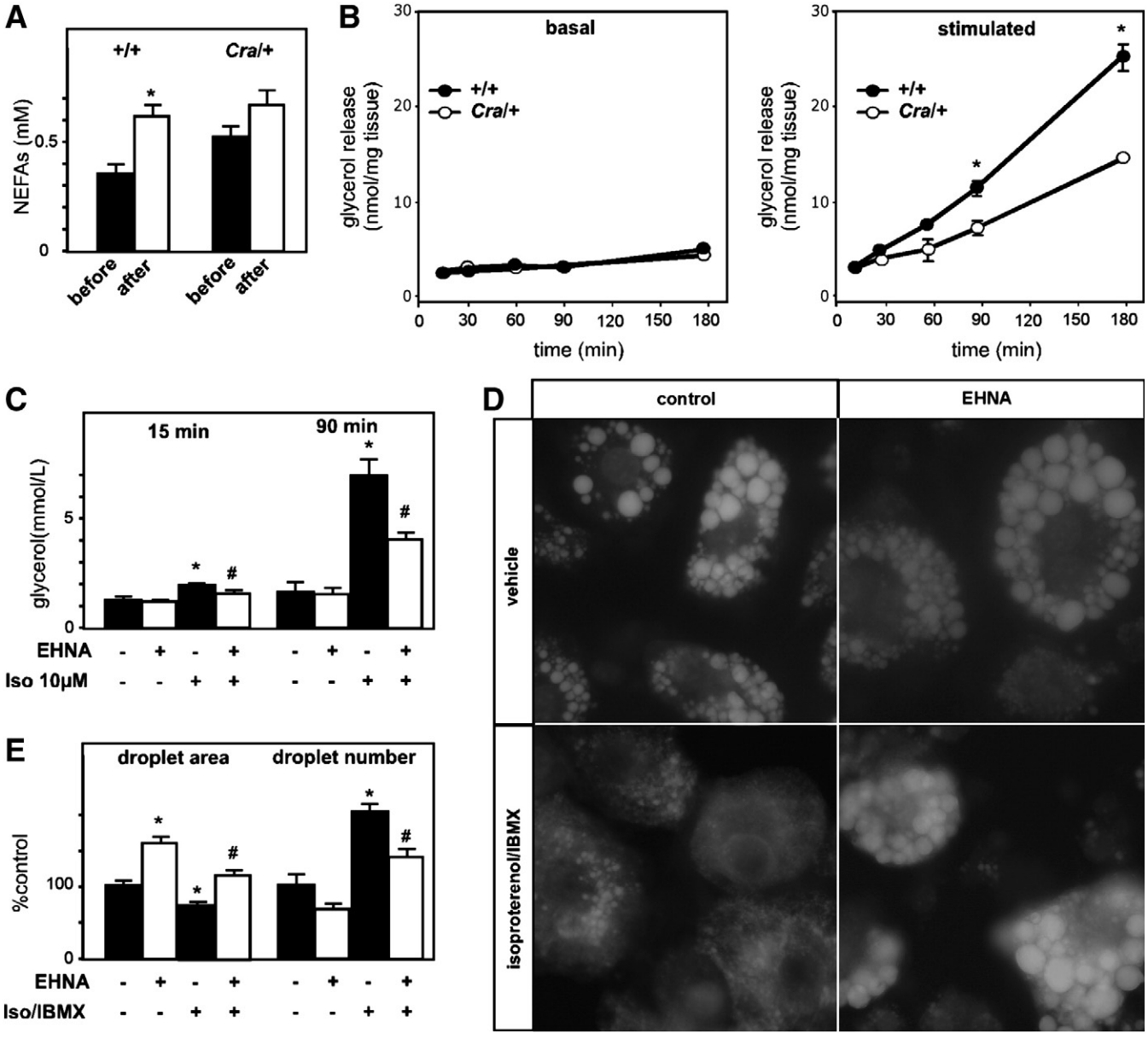

Fig. 4. Dynein involvement in adipose lipolysis. All values are indicated as mean ± SEM. (A) NEFAs levels in mmol/l before (black columns) and 20 min after (open columns) norepinephrine injection in +/+ and *Cra*/+ mice (*Cra*/+) of 4 months of age. $N = 6$ mice per group. $^{*}p<0.05$ vs. corresponding "before" condition; $^{\#}p<0.05$ vs. corresponding +/+ condition. (B) Glycerol release in nmol/mg of tissue of WAT explants from +/+ and *Cra*/+ mice of 2 months of age in basal (left panel) or stimulated by isoproterenol (right panel) condition. $^{*}p<0.05$ vs. corresponding +/+. A representative experiment out of 4 independent experiments is shown. (C) Glycerol release in nmol/mg of tissue of WAT explants from wild-type mice in basal or stimulated by isoproterenol conditions in the presence or absence of EHNA. Measures were done after 15 (left) or 90 min (right) of isoproterenol stimulation. $^{*}p<0.05$ vs. corresponding unstimulated condition; $^{\#}p<0.05$ vs. corresponding condition without EHNA. A representative experiment out of 3 independent experiments is shown. (D) Representative photomicrographs showing differentiated 3T3L1 stimulated or unstimulated with isoproterenol and the PDE inhibitor 3-isobutyl-1-methylxanthine (IBMX) in the presence or absence of EHNA. Neutral lipids are stained using Bodipy493/503 and nuclei are stained with Hoechst 33342. Note that the stimulation with isoproterenol and IBMX increases the number of droplets but strongly decreases their surface. EHNA coapplication prevented this effect. (E) Quantification of the experiments presented in panel E. $^{*}p<0.05$ vs. corresponding unstimulated condition; $^{\#}p<0.05$ vs. corresponding condition without EHNA. A representative experiment out of 3 independent experiments is shown.

already significant at 2 months of age in *Cra*/+ animals and progressed with age. Adipocytes of *Cra*/+ and *Loa*/+ mice were larger than those of their corresponding +/+ mice at 8 months of age (Fig. 1C). Before that age, mRNAs of perilipin and leptin, two genes whose expressions are correlated with adipose mass were increased in epididymal fat of 4-month-old *Cra*/+ mice (Fig. 1D) and circulating levels of leptin were increased at 4 months of age (Fig. 1E). Increased adipose mass was not due to enhanced adipogenesis since the expression of adipogenic genes such as *PPARγ*, *aP2*, and *LPL* were unchanged (Fig. 1D). Consistent with increased adiposity, adipose triglyceride lipase (ATGL) protein levels increased at 4 months of age in dynein mutant WAT, while hormone-sensitive lipase (HSL) protein levels were unchanged (Fig. 1F). Hyperadiposity might be driven by changes in energy balance of the animal, for instance, by increased energy intake or decreased energy expenditure. Despite an already detectable hyperadiposity, *Cra*/+ mice were not obese at 2 or 4 months of age, but only at 8 months of age (Fig. 2A). Resting and total energy expenditure (Fig. 2B), food intake (Fig. 2C), and spontaneous locomotor activity (Fig. 2D) were unchanged at 4 months of age. Furthermore, despite a trend towards increased lipid content, body composition of Cra/+ mice was not significantly different from that of wild-type littermates at 4 months of age (Table 1), suggesting that increased WAT deposition in these animals was compensated by decreased lipid content in other tissues. Altogether, dynein mutant mice developed increased WAT deposition, in the absence of detectable energy imbalance.

3.2. Dynein is expressed in white adipose tissue

The increase in WAT accumulation suggested that dynein was involved in adipose tissue lipid metabolism. Such an involvement could be direct, through dynein action in adipocytes, or indirect, through an impairment of CNS-derived cues. If dynein has a function in lipid metabolism in WAT, it should first be expressed in this tissue. Indeed, mRNA levels of dynein heavy chain (DHC) were detectable in WAT and many other non-CNS tissues (Fig. 3A). Moreover, mutant DHC mRNA was observed in WAT of *Cra*/+ mice (Fig. 3B). Consistent with a role in lipid metabolism, DHC mRNA levels mildly but significantly increased after 3 weeks of high-fat feeding in wild-type mice, in a manner similar to perilipin mRNA (Fig. 3C). In these experiments, the large increases in leptin mRNA (Fig. 3C) and ATGL protein levels (Fig. 3D) were consistent with efficient high-fat feeding. Thus, dynein is expressed in adipocytes and regulated by high-fat feeding, consistent with a function in lipid metabolism.

3.3. Dynein activity is required for norepinephrine-induced lipolysis

We next explored whether intrinsic defects in adipose tissue could be the cause of WAT accumulation in dynein mutant mice. The CNS mostly controls adipose tissue energy metabolism through activation of the sympathetic nervous system. Thus, if adipose tissues of *Cra*/+ mice were normal and the increased adiposity of *Cra*/+ mice was the result of a "pure" CNS defect, their responses to norepinephrine should be similar to those of +/+ littermates. Obesity is a confounding factor since development of obesity leads to blunted norepinephrine-stimulated lipolysis [18]. To take this factor into account, we performed lipolysis experiments in 4-month-old mice, i.e., an age when adiposity was increased but mice were not obese and not insulin-resistant (not shown). In WAT, sympathetic activation stimulates lipolysis leading to enhanced release of NEFAs. When +/+ mice were challenged with norepinephrine, blood levels of NEFAs almost doubled 20 min after injection. In contrast, *Cra*/+ mice injected in parallel showed only a non-significant 25% increase in NEFAs levels (Fig. 4A). In order to directly measure lipolysis, we cultured WAT explants of +/+ and *Cra*/+ mice at 4 months of age, stimulated them with norepinephrine, and measured glycerol in the culture medium as lipolysis index. As shown in Fig. 4B, lipolysis was unchanged in basal conditions, but after norepinephrine stimulation, the lipolytic response was twofold less in *Cra*/+ than in +/+ mice. Similar results were obtained by standardizing either by tissue weight or protein content (not shown). We next sought to determine whether pharmacological inhibition of dynein ATPase activity also inhibited lipolysis. For this, we used explants of WAT from wild-type animals and treated them or not with EHNA, a widely documented inhibitor of dynein ATPase activity [19,20]. Consistent with the results obtained in *Cra*/+ mice, basal lipolytic activity of WAT explants was unchanged by EHNA treatment while norepinephrine-stimulated lipolysis was completely blunted by EHNA coapplication (Fig. 4C). To further document this point, we turned to the differentiated 3T3L1 cell line. In these cells, multiple lipid droplets are readily observable in the cytosol. The diameter of lipid droplets increased with EHNA treatment (Fig. 4D), suggesting that dynein inhibition resulted in increased lipid storage in these cells. Furthermore, the decrease in droplet diameter elicited by isoproterenol treatment was potently inhibited by EHNA coapplication (Fig. 4D–E). Thus, here again, dynein ATPase activity was required for adipocyte lipolysis.

3.4. Decreased lipolysis in dynein mutant WAT is associated with defective β-adrenergic signaling and due to increased oxidative stress

To define the mechanisms underlying defective lipolysis in dynein mutant mice, we first studied β-adrenergic signaling. The expressions of HSL and β2 adrenergic receptor were roughly normal in *Cra*/+ WAT (Fig. S1), and HSL protein levels were unchanged (Fig. 1E). Upon isoproterenol stimulation, WAT explants of *Cra*/+ mice showed blunted phosphorylation of HSL (Fig. 5A–B). PKA activity, as evaluated by PKA substrate immunoreactivity, appeared, however, not significantly decreased (Fig. 5A–B). Thus, dynein mutation triggered specifically abnormal PKA-mediated phosphorylation of HSL. However, direct adenylate cyclase activation by forskolin did not correct lipolysis deficiency (Fig. S2), showing that the defect was independent of adenylate cyclase activation. Beta-adrenergic stimulation is known to modulate hydrogen peroxide production in adipocytes through PKA-independent pathways [21,22]. Interestingly, hydrogen peroxide is known to inhibit norepinephrine-induced lipolysis [23,24], and drugs interfering with the stability of microtubules, i.e., the dynein railroad tracks, are known to increase oxidative stress through NADPH oxidase activation [25,26]. To directly study whether dynein mutation might lead to exacerbated oxidative stress, we measured H_2O_2 production in response to norepinephrine stimulation. Consistent with previous

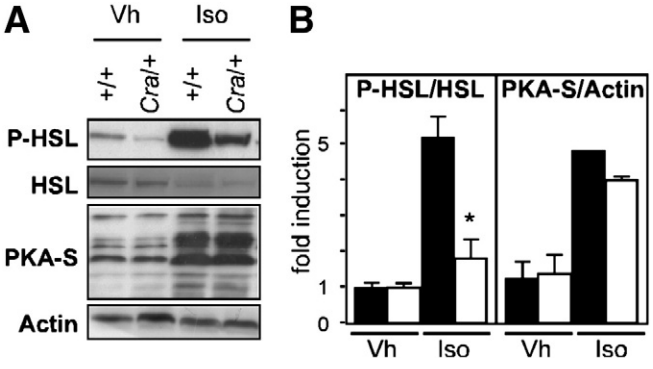

Fig. 5. Defective lipolysis in dynein mutant WAT is associated with defective β-adrenergic signaling. All values are indicated as mean ± SEM. Wild-type mice (+/+) are indicated using black symbols and dynein mutant mice (*Cra*/+) using open symbols. (A) Representative Western blotting of phosphorylated Ser 563 hormone-sensitive lipase (P-HSL), total hormone-sensitive lipase (HSL), phosphorylated PKA substrate immunoreactivity (PKA-S), and actin of +/+ and *Cra*/+ mice WAT explants treated for 3 h with (Iso) or without (vh, vehicle) 10 μM of isoproterenol. (B) Quantification of the experiments presented in panel A. Four independent experiments were performed. *$p<0.05$ vs. +/+.

works, H_2O_2 was decreased in +/+ mice after norepinephrine stimulation (Fig. 6A). H_2O_2 was less in basal conditions in *Cra*/+ WAT explants, but potently stimulated after isoproterenol stimulation (Fig. 6A). In WAT, oxidative stress is largely NADPH oxidase-dependent [27] and inhibition of NADPH oxidase with apocynin completely abolished H_2O_2 production in both *Cra*/+ and +/+ mice (Fig. 6A). To further document the existence of oxidative stress in *Cra*/+ WAT after norepinephrine stimulation, we treated WAT explants with the superoxide probe hydroethidine, which yields a nuclear fluorescent staining when superoxide is produced. Upon norepinephrine treatment, nuclei of *Cra*/+ WAT became brightly fluorescent, an event not observed in +/+ WAT explants (Fig. 6C). We next measured the expression levels of NADPH oxidase subunits (gp47 and gp91) in WAT, as well as known antioxidant enzymes (SOD1 and glutathione peroxidase), and NFkappaB targets induced after oxidative stress (MCP-1 and IL6). All these genes were intensely up regulated in *Cra*/+ mice WAT at 4 months of age (Fig. 6B). Although these upregulations do not necessarily mean that the corresponding proteins are increased, their coordinations provide indirect evidence of a potent antioxidant response. Last, in order to determine whether the defect in lipolysis was due to NADPH-oxidase-dependent oxidative stress, we treated WAT explants with apocynin and followed glycerol release upon isoproterenol stimulation. In these experiments, apocynin partially reverted *Cra*/+ defect in stimulated lipolysis (Fig. 6D) and restored HSL phosphorylation (Fig. 6E). Thus, dynein mutation limits stimulated lipolysis through a deregulation of endogenous oxidative stress.

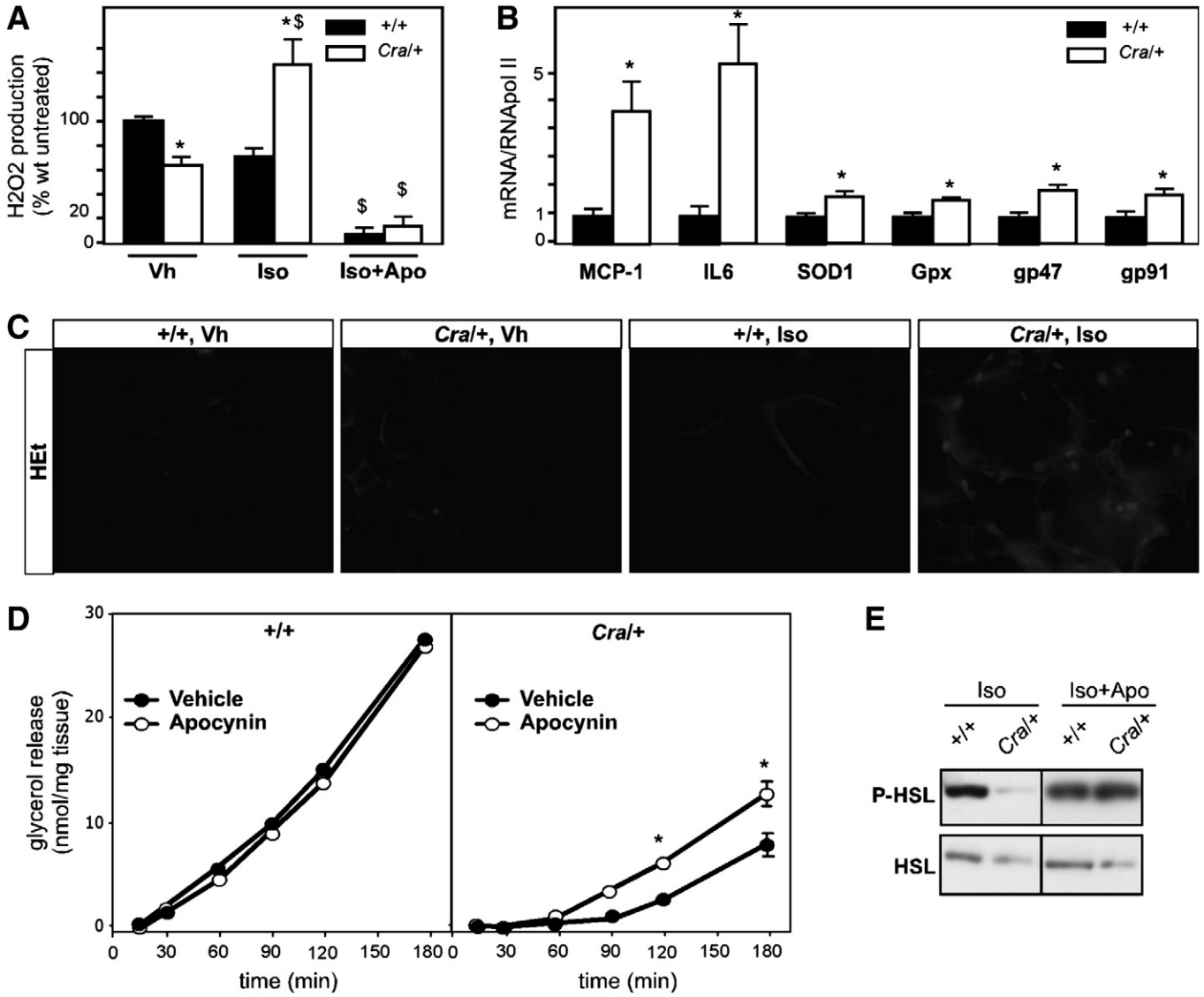

Fig. 6. Defective lipolysis in dynein mutant WAT is due to oxidative stress leading to defective β-adrenergic signaling. All values are indicated as mean ± SEM. Wild-type mice (+/+) are indicated using black symbols and dynein mutant mice (*Cra*/+) using open symbols. (A) H_2O_2 production in +/+ and *Cra*/+ WAT explants after vehicle (Vh), 10 μM isoproterenol (Iso), and isoproterenol + 10 μM apocynin (Iso+Apo) treatments. $^*p<0.05$ vs. corresponding wild type, $^\$p<0.05$ vs. corresponding Iso condition. (B) mRNA levels of monocyte chemotactic protein 1 (MCP-1), interleukin-6 (IL-6), Cu/Zn superoxide dismutase (SOD1), glutathione peroxidase (Gpx), NAPDH oxidase subunits gp47 (gp47) and gp91 (gp91) in white adipose tissue from +/+ and *Cra*/+ mice at 4 months of age. $^*p<0.05$ vs. +/+ ($n=5$–7 mice per group). (C) Hydroethidine staining in +/+ and *Cra*/+ WAT explants 15-min exposure to 10 μM isoproterenol or vehicle. Note that a number of nuclei are brightly stained in treated *Cra*/+ WAT showing that isoproterenol treatment increased superoxide production. (D) Glycerol release in nmol/mg of tissue of white adipose tissue explants stimulated by 10 μM isoproterenol from +/+ (left panel) and *Cra*/+ (right panel) mice in the presence (open circles) or absence (black circles) of 10 μM apocynin. $^*p<0.05$ vs. corresponding untreated condition. A representative experiment out of 3 independent experiments is shown. (E) Representative Western blotting of phosphorylated Ser 563 hormone-sensitive lipase (P-HSL), and total hormone-sensitive lipase (HSL), of +/+ and *Cra*/+ mice WAT explants treated for 3 h with 10 μM isoproterenol in the absence (Iso) or presence (Iso + Apo) of 10 μM apocynin.

3.5. Defective thermogenesis in dynein mutant mice

We next sought to determine whether the defect in lipolysis was restricted to the WAT. The interscapular brown adipose tissue (BAT) was paler (not shown) and increased in size at 4 months of age (Fig. 7A), and brown adipocytes accumulated fat as observed on histological sections of both *Cra*/+ and *Loa*/+ BAT (Fig. 7B). This abnormal BAT phenotype was not due to transcriptional downregulation of UCP1 since mRNA levels of both UCP1 and PGC1α, one of its key activators, were unchanged at 4 months of age. *Cra*/+ mice displayed normal rectal temperature at 4 months of age but were hypothermic at 8 months of age (Fig. 8A). BAT function was, however, already abnormal at 4 months of age since a 4-h cold challenge leads to hypothermia in *Cra*/+ mice in 4- and 8-month-old mice (Fig. 8B and data not shown). Furthermore, 4-month-old *Cra*/+ mice were unable to increase energy expenditure upon cold at levels similar to +/+ mice (Fig. 8C). We reasoned that the BAT defect resulted also from a decreased response to norepinephrine. To test this hypothesis, we challenged *Cra*/+ mice with norepinephrine and measured their oxygen consumption (Fig. 8D). The burst in oxygen consumption after norepinephrine injection reflects sympathetic-like BAT activation. We observed that saline injection led to a transient increase in oxygen consumption during the first 15 min after the injection, an increase probably due to the stress response induced by animal handling. However, the increase in oxygen consumption was sustained at least 30 min after norepinephrine injection (Fig. 8D). Most interestingly, norepinephrine-evoked oxygen consumption was strongly decreased in *Cra*/+ mice as compared with +/+ littermates (Fig. 8E). In all, our results obtained *in vivo*, *ex vivo*, and *in vitro* all converge to ascertain a key role to dynein in the control of adipose tissue lipolysis underlying lipid accumulation in the WAT and dysfunctional BAT-mediated thermogenesis. These defects are intrinsic to adipose tissues and independent of other CNS-linked consequences of dynein mutation.

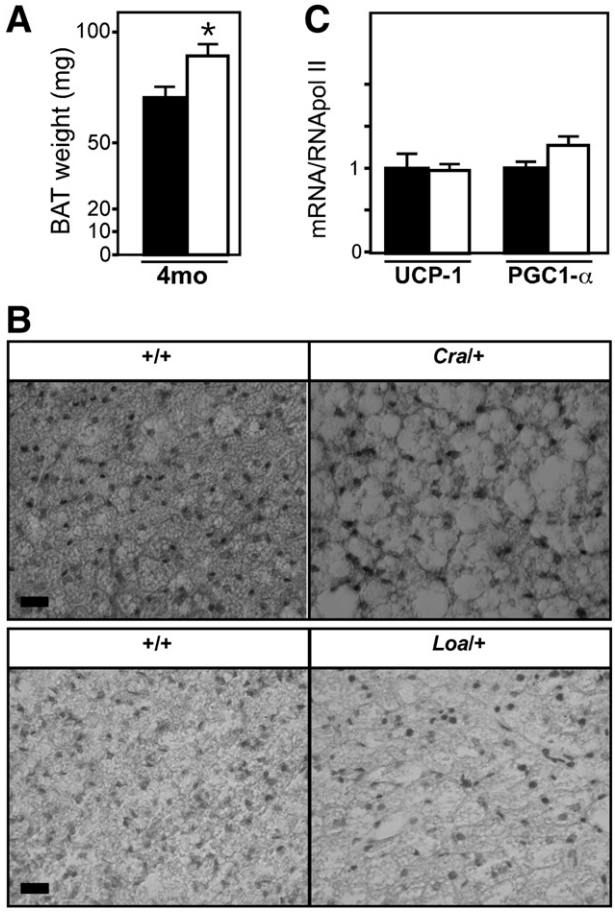

Fig. 7. Defective brown adipose tissue morphology in dynein mutant mice. (A) Interscapular brown adipose tissue (BAT) weight of wild-type (+/+, black columns) and dynein mutant (*Cra*/+, empty columns) mice at 4 months (4mo) of age. $^{*}p<0.05$ vs. +/+ ($n=6$–8 mice per group). (B) Representative photomicrograph showing BAT sections of 8-month-old *Cra*/+ (upper panels) and 5-month-old *Loa*/+ (lower panels) mice and their corresponding +/+ mice stained with hematoxylin and eosin. Note the prominent appearance of fat vesicles. Scale bar = 25 μm. (C) mRNA levels of mitochondrial uncoupling protein 1 (UCP1) and PPARγ-coactivator 1 α (PGC1α) in the BAT from wild type (+/+, black columns) and dynein mutant (*Cra*/+, empty columns) at 4 months of age. $^{*}p<0.05$ vs. +/+ ($n=5$–7 mice per group).

3.6. Dynein mutation decreases levels of huntingtin in the WAT

The previous results obtained in WAT and BAT of dynein mutant animals are reminiscent of HD-associated defects observed in animal models of HD [13,14,28,29]. To strengthen the analogy between the animal models, we studied the expression levels of huntingtin and its associated protein HAP-1 [30,31] in WAT of dynein mutant mice. Huntingtin, but not HAP-1, was expressed at significant levels in WAT (results not shown) and huntingtin mRNA levels appeared unchanged in WAT of 4-month-old dynein mutant mice (Fig. 9A). Interestingly, however, protein levels of full-length huntingtin were decreased in the WAT of 4-month-old dynein mutant mice (Fig. 9B). Thus, the dynein mutation led to decreased huntingtin protein levels in adult WAT.

4. Discussion

The molecular motor dynein is ubiquitously expressed in adult animals, including in post-mitotic cells, yet its role remains obscure in adult cells other than neurons. Our results document a previously unknown function for dynein in adipose tissue response to norepinephrine and lipolysis. The dynein-mutant-associated defect in lipolysis was due to a dysfunctional β-adrenergic signaling and appeared to be, at least in part, dependent on NADPH-oxidase-derived oxidative stress. These findings define dynein as a novel potential actor in energy homeostasis that could be of interest for type 2 diabetes. Furthermore, the peripheral phenotype described here in dynein mutant mice is strikingly similar to that of various animal models of Huntington's disease, further supporting the idea that dynein and huntingtin are functionally linked.

4.1. The adipocyte phenotype of dynein mutant mice is independent of the central nervous system

Dynein function has been largely studied in the CNS, yet this motor is ubiquitously expressed. We show here that dynein function is critical in the response of adipose tissues to norepinephrine. This requirement is due to a function of dynein in adipocytes themselves and is not a secondary consequence of a CNS abnormality in dynein mutant mice. Several lines of evidence support this claim. First, dynein is expressed in adipose tissue and regulated in a manner consistent with a function in lipid metabolism. Second, the WAT phenotype occurs in early adulthood, long before neurodegeneration was thought to occur [4]. Third, the defect in lipolysis is recapitulated *ex vivo*, in the absence of CNS-derived cues and *in vitro* upon chemical inhibition of dynein. Fourth, this defect occurred in mice with normal energy balance, most notably with normal energy intake and energy expenditure. This, however, does not fully exclude a CNS influence on the adipose phenotype. The generation of conditional knock out animals will be a necessary step to solve this question.

4.2. Dynein is required at several steps in lipid metabolism

The dynein motor has been firmly established as a major actor in lipid droplet formation [32–36]. First, an RNAi-based functional screen revealed that dynein knockdown resulted in strikingly diminished lipid accumulation in *Drosophila* cells [36]. Furthermore, dynein is a component of mammalian lipid droplets [32] and appears required for the formation of

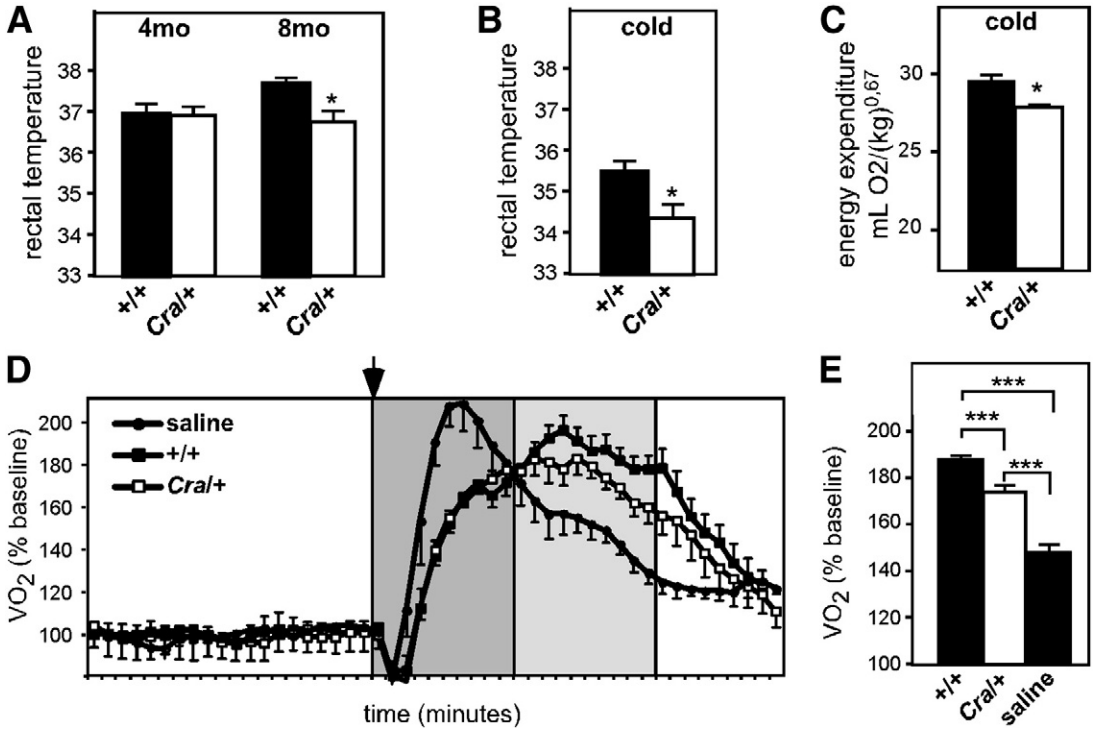

Fig. 8. Defective brown adipose tissue thermogenic function in dynein mutant mice. (A) Rectal temperatures in basal conditions in 4 (4mo)- and 8 (8mo)-month-old wild-type (+/+, black columns) and dynein mutant (*Cra*/+, empty columns) mice. $N=8$ per group. $^{*}p<0.05$ vs. corresponding +/+. (B) Rectal temperatures after a 4-h cold challenge (7 °C) in 4-month-old wild-type (+/+, black columns) and dynein mutant (*Cra*/+, empty columns) mice. $N=8$ per group. $^{*}p<0.05$ vs. corresponding +/+. (C) Total energy expenditure of 4-month-old wild-type (+/+, black columns) and dynein mutant (*Cra*/+, empty columns) mice during a 24-h cold challenge (7 °C). $N=8$ per group. $^{*}p<0.05$ vs. +/+. (D–E) Norepinephrine challenge: energy expenditure expressed in percentage of the baseline for +/+ (black squares), *Cra*/+ (open squares), and mice injected with saline (vehicle, black circles). Norepinephrine was injected intraperitoneally at t0 (arrow), and energy expenditure was measured during 1 h after the injection. The first 15 min (dark grey) was discarded for the quantification due to the strong effect of the injection *per se* (see the strong increase in energy expenditure in vehicle-injected mice). Measures from 15 to 30 min (light grey) were used for the quantification in panel E. $^{***}p<0.001$ vs. condition shown.

these organelles [32–34]. Indeed, chemical inhibition of dynein in differentiated 3T3L1 cells increased the size of lipid droplets not only in isoproterenol treated cells but also in basal conditions, consistent with dynein involvement in lipid droplet trafficking [32,34]. This function of dynein resembles that demonstrated for perilipin [37] or caveolin 1 [38], both of these proteins being involved in lipid droplet formation in adipocytes. Nevertheless, and contrary to either perilipin −/− or caveolin1 −/− mice, dynein mutant mice were not lean but showed strikingly enhanced adipose fat pads with strongly increased WAT weight long before obesity was observed and WAT explants of dynein mutant mice did not show changes in basal lipolysis. This suggests that lipid droplet formation and protection of lipids from lipases were not changed by the dynein mutation, consistent with the fact that dynein mutation does not significantly impair housekeeping functions of dynein but rather decreases dynein transport upon cellular stress [4]. Despite normal basal lipolysis, Cra/+ WAT showed decreased ability to provide an adequate lipolytic response to norepinephrine. Importantly, BAT norepinephrine response was also defective and underlay the defect in thermogenesis observed in mutant animals. Thus, a first important result of this study is that, besides its known role in lipid droplet formation, dynein is involved in adipose tissue response to norepinephrine.

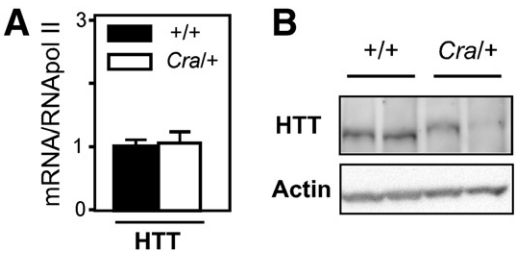

Fig. 9. Decreased huntingtin protein levels in dynein mutant WAT. (A) mRNA levels of huntingtin (HTT) in the WAT from wild-type (+/+, black columns) and dynein mutant (*Cra*/+, empty columns) at 4 months of age. No significant difference is observed. (B) Representative Western blotting of huntingtin (HTT) and actin in the epididimary WAT from 4-month-old +/+ and *Cra*/+ mice.

4.3. Mechanisms underlying dynein involvement in stimulated lipolysis

We next defined the mechanisms underlying dynein function in stimulated lipolysis. First, dynein mutation blunted the effects of norepinephrine on HSL phosphorylation. This signaling defect was not due to strongly impaired PKA activation but rather to a selective inhibition of PKA-mediated HSL phosphorylation. Two lines of evidence suggested that dynein did not impair the classical cAMP/PKA axis after norepinephrine stimulation: first, PKA activity appeared only mildly decreased in Cra/+ WAT after stimulation. Second, direct activation of adenylate cyclase by forskolin did not correct the lipolysis defect, suggesting that the defect was either downstream adenylate cyclase or affecting other pathways elicited by the beta-adrenergic receptors. A number of accessory pathways have been described after beta-adrenergic stimulation. Among them, we chose to focus on NADPH oxidase oxidative stress production. Indeed, NADPH-oxidase-dependent oxidative stress has been shown to participate in several aspects of the transduction pathway of beta-adrenergic receptors, independently of PKA [22,39] although whether norepinephrine actually increases [22,24] or decreases [21] oxidative stress production in adipocytes remains controversial. Furthermore, NADPH activation has been shown to be downstream the cellular effects of microtubules depolymerising drugs [25,26]. Here, we observed that norepinephrine decreased H_2O_2 production in wild-type adipocytes, a result similar to that of Krieger and collaborators [21]. Contrasting with this, H_2O_2 production was

potently increased in *Cra*/+ adipocytes suggesting that an inhibitory mechanism was lost in dynein mutant WAT. Consistent with increased oxidative stress, superoxide production in response to norepinephrine was noticeable in dynein mutant adipocytes and we observed an oxidative stress-like transcriptional fingerprint in WAT. Interestingly, previous work has indicated that NADPH oxidase inhibition after beta-adrenergic stimulation was due to the beta-gamma subunits of G(s) protein [21] and that the dynein light chain Tctex1 is known to modulate G protein beta gamma subunits [40]. Another dynein light chain, LC8, was involved in the attenuation of NFkappaB signaling after NADPH oxidase stimulation by oxidative stress [41]. Whether dynein mutation leads to abnormal function of Tctex1 and/or LC8 underlying increased NADPH-oxidase-dependent oxidative stress in *Cra*/+ WAT will require further work. Our study, however, shows that NADPH-oxidase ROS production was responsible for at least part of the inhibition of lipolysis since HSL phosphorylation was restored by apocynin, a specific NAPDH oxidase inhibitor [42] and since apocynin treatment also reverted the defect in lipolysis.

4.4. Potential consequences for Huntington's disease

Dynein is especially known for its involvement in neurodegenerative diseases, especially in motor neuron diseases and in Huntington's disease (HD). More specifically for HD, mutant Huntingtin decreases dynein activity, and this might be crucial for the pathogenesis [9,10]. Interestingly, our current results show that huntingtin protein levels are decreased in dynein mutant mice. The mechanisms underlying this defect, as well as its relationship with the phenotype described here, are still elusive. It is striking to note that a very similar metabolic phenotype was observed in HD animal models (for review, see Refs. [43–45]). Notably, R6/2 transgenic mice show increased adiposity [14,28], in the absence of obesity [14,28,29]. Adipose tissue of R6/2 mice show decreased isoproterenol-stimulated lipolysis [14] and brown adipose tissue-mediated thermogenesis was profoundly impaired [13]. In all, the peripheral phenotype observed in R6/2 mice was strikingly similar to dynein mutant phenotype, suggesting that common pathways, for instance, through modification of PGC1alpha function [13,28], might be at work upon dynein mutation and mutant huntingtin expression. To our knowledge, similar studies in HD adipose tissues are lacking, although a large consensus exists that HD leads to a widespread pathology besides CNS pathology [46].

5. Conclusions

In all, our study provides the first *in vivo* evidence of a key role for a molecular motor in adipose tissue physiology through its regulatory role on reactive oxygen species production after norepinephrine stimulation. Exploration of the contribution of dynein and its interacting proteins to human diabetes and metabolic syndrome is warranted. Our study also provides further support for decreased dynein function as a potential mechanism of HD.

Supplementary materials related to this article can be found online at doi:10.1016/j.bbadis.2010.09.009.

Acknowledgments

The study was supported by grants from the ALS association (2008) and Association pour la Recherche sur la Sclerose Laterale Amyotrophique (A.R.S.) to L.D. (2007) and A.R.S. to J.L.G.D.A (2006); Association Francaise contre les Myopathies, A.R.S. and Association pour la Recherche et le Developpement de Moyens de Lutte contre les Maladies Neurodegeneratives to J.P.L.; KFO142 for ACL; J.L.G.D.A. is the recipient of chaire INSERM/Université de Strasbourg.

References

[1] E. Chevalier-Larsen, E.L. Holzbaur, Axonal transport and neurodegenerative disease, Biochim. Biophys. Acta 1762 (2006) 1094–1108.
[2] Y. Zheng, J. Wildonger, B. Ye, Y. Zhang, A. Kita, S.H. Younger, S. Zimmerman, L.Y. Jan, Y.N. Jan, Dynein is required for polarized dendritic transport and uniform microtubule orientation in axons, Nat. Cell Biol. 10 (2008) 1172–1180.
[3] A. Harada, Y. Takei, Y. Kanai, Y. Tanaka, S. Nonaka, N. Hirokawa, Golgi vesiculation and lysosome dispersion in cells lacking cytoplasmic dynein, J. Cell Biol. 141 (1998) 51–59.
[4] M. Hafezparast, R. Klocke, C. Ruhrberg, A. Marquardt, A. Ahmad-Annuar, S. Bowen, G. Lalli, A.S. Witherden, H. Hummerich, S. Nicholson, P.J. Morgan, R. Oozageer, J.V. Priestley, S. Averill, V.R. King, S. Ball, J. Peters, T. Toda, A. Yamamoto, Y. Hiraoka, M. Augustin, D. Korthaus, S. Wattler, P. Wabnitz, C. Dickneite, S. Lampel, F. Boehme, G. Peraus, A. Popp, M. Rudelius, J. Schlegel, H. Fuchs, M. Hrabe de Angelis, G. Schiavo, D.T. Shima, A.P. Russ, G. Stumm, J.E. Martin, E.M. Fisher, Mutations in dynein link motor neuron degeneration to defects in retrograde transport, Science 300 (2003) 808–812.
[5] E. Perlson, G.B. Jeong, J.L. Ross, R. Dixit, K.E. Wallace, R.G. Kalb, E.L. Holzbaur, A switch in retrograde signaling from survival to stress in rapid-onset neurodegeneration, J. Neurosci. 29 (2009) 9903–9917.
[6] H.S. Ilieva, K. Yamanaka, S. Malkmus, O. Kakinohana, T. Yaksh, M. Marsala, D.W. Cleveland, Mutant dynein (Loa) triggers proprioceptive axon loss that extends survival only in the SOD1 ALS model with highest motor neuron death, Proc. Natl. Acad. Sci. U. S. A. 105 (2008) 12599–12604.
[7] L. Dupuis, A. Fergani, K.E. Braunstein, J. Eschbach, N. Holl, F. Rene, J.L. Gonzalez De Aguilar, B. Zoerner, B. Schwalenstocker, A.C. Ludolph, J.P. Loeffler, Mice with a mutation in the dynein heavy chain 1 gene display sensory neuropathy but lack motor neuron disease, Exp. Neurol. 215 (2009) 146–152.
[8] X.J. Chen, E.N. Levedakou, K.J. Millen, R.L. Wollmann, B. Soliven, B. Popko, Proprioceptive sensory neuropathy in mice with a mutation in the cytoplasmic Dynein heavy chain 1 gene, J. Neurosci. 27 (2007) 14515–14524.
[9] J.P. Caviston, J.L. Ross, S.M. Antony, M. Tokito, E.L. Holzbaur, Huntingtin facilitates dynein/dynactin-mediated vesicle transport, Proc. Natl. Acad. Sci. U. S. A. 104 (2007) 10045–10050.
[10] L.R. Gauthier, B.C. Charrin, M. Borrell-Pages, J.P. Dompierre, H. Rangone, F.P. Cordelieres, J. De Mey, M.E. MacDonald, V. Lessmann, S. Humbert, F. Saudou, Huntingtin controls neurotrophic support and survival of neurons by enhancing BDNF vesicular transport along microtubules, Cell 118 (2004) 127–138.
[11] K.E. Braunstein, J. Eschbach, K. Rona-Voros, R. Soylu, E. Mikrouli, Y. Larmet, F. Rene, J.L. Gonzalez De Aguilar, J.P. Loeffler, H.P. Muller, S. Bucher, T. Kaulisch, H.G. Niessen, J. Tillmanns, K. Fischer, B. Schwalenstocker, J. Kassubek, B. Pichler, D. Stiller, A. Petersen, A.C. Ludolph, L. Dupuis, A point mutation in the dynein heavy chain gene leads to striatal atrophy and compromises neurite outgrowth of striatal neurons, Hum. Mol. Genet. (2010), doi:10.1093/hmg/ddq1361.
[12] A. Petersen, M. Bjorkqvist, Hypothalamic-endocrine aspects in Huntington's disease, Eur. J. Neurosci. 24 (2006) 961–967.
[13] P. Weydt, V.V. Pineda, A.E. Torrence, R.T. Libby, T.F. Satterfield, E.R. Lazarowski, M.L. Gilbert, G.J. Morton, T.K. Bammler, A.D. Strand, L. Cui, R.P. Beyer, C.N. Easley, A.C. Smith, D. Krainc, S. Luquet, I.R. Sweet, M.W. Schwartz, A.R. La Spada, Thermoregulatory and metabolic defects in Huntington's disease transgenic mice implicate PGC-1alpha in Huntington's disease neurodegeneration, Cell Metab. 4 (2006) 349–362.
[14] J.N. Fain, N.A. Del Mar, C.A. Meade, A. Reiner, D. Goldowitz, Abnormalities in the functioning of adipocytes from R6/2 mice that are transgenic for the Huntington's disease mutation, Hum. Mol. Genet. 10 (2001) 145–152.
[15] L. Dupuis, H. Oudart, F. Rene, J.L. Gonzalez de Aguilar, J.P. Loeffler, Evidence for defective energy homeostasis in amyotrophic lateral sclerosis: benefit of a high-energy diet in a transgenic mouse model, Proc. Natl. Acad. Sci. U. S. A. 101 (2004) 11159–11164.
[16] J. Folch, M. Lees, G.H. Sloane Stanley, A simple method for the isolation and purification of total lipides from animal tissues, J. Biol. Chem. 226 (1957) 497–509.
[17] W.S. Rasband, ImageJ, http://rsb.info.nih.gov/ij/, U.S. National Institutes of Health, Bethesda, Maryland, U.S.A., 1997-2008.
[18] D. Langin, A. Dicker, G. Tavernier, J. Hoffstedt, A. Mairal, M. Ryden, E. Arner, A. Sicard, C.M. Jenkins, N. Viguerie, V. van Harmelen, R.W. Gross, C. Holm, P. Arner, Adipocyte lipases and defect of lipolysis in human obesity, Diabetes 54 (2005) 3190–3197.
[19] B. Ravikumar, A. Acevedo-Arozena, S. Imarisio, Z. Berger, C. Vacher, C.J. O'Kane, S.D. Brown, D.C. Rubinsztein, Dynein mutations impair autophagic clearance of aggregate-prone proteins, Nat. Genet. 37 (2005) 771–776.
[20] P. Ekstrom, M. Kanje, Inhibition of fast axonal transport by erythro-9-[3-(2-hydroxynonyl)]adenine, J. Neurochem. 43 (1984) 1342–1345.
[21] H.I. Krieger-Brauer, P.K. Medda, B. Sattel, H. Kather, Inhibitory effect of isoproterenol on NADPH-dependent H(2)O(2) generation in human adipocyte plasma membranes is mediated by betagamma-subunits derived from G(s), J. Biol. Chem. 275 (2000) 2486–2490.
[22] N.H. Moniri, Y. Daaka, Agonist-stimulated reactive oxygen species formation regulates beta2-adrenergic receptor signal transduction, Biochem. Pharmacol. 74 (2007) 64–73.
[23] G. Muller, S. Wied, S. Over, W. Frick, Inhibition of lipolysis by palmitate, H_2O_2 and the sulfonylurea drug, glimepiride, in rat adipocytes depends on cAMP degradation by lipid droplets, Biochemistry 47 (2008) 1259–1273.
[24] M.S. Gauthier, H. Miyoshi, S.C. Souza, J.M. Cacicedo, A.K. Saha, A.S. Greenberg, N.B. Ruderman, AMP-activated protein kinase is activated as a consequence of lipolysis in the adipocyte: potential mechanism and physiological relevance, J. Biol. Chem. 283 (2008) 16514–16524.

[25] J. Alexandre, Y. Hu, W. Lu, H. Pelicano, P. Huang, Novel action of paclitaxel against cancer cells: bystander effect mediated by reactive oxygen species, Cancer Res. 67 (2007) 3512–3517.
[26] H.J. Jang, S. Hwang, K.Y. Cho, K. Kim do, K.O. Chay, J.K. Kim, Taxol induces oxidative neuronal cell death by enhancing the activity of NADPH oxidase in mouse cortical cultures, Neurosci. Lett. 443 (2008) 17–22.
[27] S. Furukawa, T. Fujita, M. Shimabukuro, M. Iwaki, Y. Yamada, Y. Nakajima, O. Nakayama, M. Makishima, M. Matsuda, I. Shimomura, Increased oxidative stress in obesity and its impact on metabolic syndrome, J. Clin. Invest. 114 (2004) 1752–1761.
[28] J. Phan, M.A. Hickey, P. Zhang, M.F. Chesselet, K. Reue, Adipose tissue dysfunction tracks disease progression in two Huntington's disease mouse models, Hum. Mol. Genet. 18 (2009) 1006–1016.
[29] J.M. van der Burg, K. Bacos, N.I. Wood, A. Lindqvist, N. Wierup, B. Woodman, J.I. Wamsteeker, R. Smith, T. Deierborg, M.J. Kuhar, G.P. Bates, H. Mulder, C. Erlanson-Albertsson, A.J. Morton, P. Brundin, A. Petersen, M. Bjorkqvist, Increased metabolism in the R6/2 mouse model of Huntington's disease, Neurobiol. Dis. 29 (2008) 41–51.
[30] S. Engelender, A.H. Sharp, V. Colomer, M.K. Tokito, A. Lanahan, P. Worley, E.L. Holzbaur, C.A. Ross, Huntingtin-associated protein 1 (HAP1) interacts with the p150Glued subunit of dynactin, Hum. Mol. Genet. 6 (1997) 2205–2212.
[31] X.J. Li, S.H. Li, A.H. Sharp, F.C. Nucifora Jr., G. Schilling, A. Lanahan, P. Worley, S.H. Snyder, C.A. Ross, A huntingtin-associated protein enriched in brain with implications for pathology, Nature 378 (1995) 398–402.
[32] L. Andersson, P. Bostrom, J. Ericson, M. Rutberg, B. Magnusson, D. Marchesan, M. Ruiz, L. Asp, P. Huang, M.A. Frohman, J. Boren, S.O. Olofsson, PLD1 and ERK2 regulate cytosolic lipid droplet formation, J. Cell Sci. 119 (2006) 2246–2257.
[33] P. Bostrom, L. Andersson, M. Rutberg, J. Perman, U. Lidberg, B.R. Johansson, J. Fernandez-Rodriguez, J. Ericson, T. Nilsson, J. Boren, S.O. Olofsson, SNARE proteins mediate fusion between cytosolic lipid droplets and are implicated in insulin sensitivity, Nat. Cell Biol. 9 (2007) 1286–1293.
[34] P. Bostrom, M. Rutberg, J. Ericsson, P. Holmdahl, L. Andersson, M.A. Frohman, J. Boren, S.O. Olofsson, Cytosolic lipid droplets increase in size by microtubule-dependent complex formation, Arterioscler. Thromb. Vasc. Biol. 25 (2005) 1945–1951.
[35] S.P. Gross, M.A. Welte, S.M. Block, E.F. Wieschaus, Dynein-mediated cargo transport in vivo. A switch controls travel distance, J. Cell Biol. 148 (2000) 945–956.
[36] Y. Guo, T.C. Walther, M. Rao, N. Stuurman, G. Goshima, K. Terayama, J.S. Wong, R.D. Vale, P. Walter, R.V. Farese, Functional genomic screen reveals genes involved in lipid-droplet formation and utilization, Nature 453 (2008) 657–661.
[37] J.T. Tansey, C. Sztalryd, J. Gruia-Gray, D.L. Roush, J.V. Zee, O. Gavrilova, M.L. Reitman, C.X. Deng, C. Li, A.R. Kimmel, C. Londos, Perilipin ablation results in a lean mouse with aberrant adipocyte lipolysis, enhanced leptin production, and resistance to diet-induced obesity, Proc. Natl. Acad. Sci. U. S. A. 98 (2001) 6494–6499.
[38] A.W. Cohen, B. Razani, W. Schubert, T.M. Williams, X.B. Wang, P. Iyengar, D.L. Brasaemle, P.E. Scherer, M.P. Lisanti, Role of caveolin-1 in the modulation of lipolysis and lipid droplet formation, Diabetes 53 (2004) 1261–1270.
[39] K. Gong, Z. Li, M. Xu, J. Du, Z. Lv, Y. Zhang, A novel protein kinase A-independent, beta-arrestin-1-dependent signaling pathway for p38 mitogen-activated protein kinase activation by beta2-adrenergic receptors, J. Biol. Chem. 283 (2008) 29028–29036.
[40] P. Sachdev, S. Menon, D.B. Kastner, J.Z. Chuang, T.Y. Yeh, C. Conde, A. Caceres, C.H. Sung, T.P. Sakmar, G protein beta gamma subunit interaction with the dynein light-chain component Tctex-1 regulates neurite outgrowth, EMBO J. 26 (2007) 2621–2632.
[41] Y. Jung, H. Kim, S.H. Min, S.G. Rhee, W. Jeong, Dynein light chain LC8 negatively regulates NF-kappaB through the redox-dependent interaction with IkappaBalpha, J. Biol. Chem. 283 (2008) 23863–23871.
[42] J. Stefanska, R. Pawliczak, Apocynin: molecular aptitudes, Mediators Inflamm. 2008 (2008) 106507.
[43] R.J. Ferrante, Mouse models of Huntington's disease and methodological considerations for therapeutic trials, Biochim. Biophys. Acta 1792 (2009) 506–520.
[44] A. Petersen, S. Hult, D. Kirik, Huntington's disease—new perspectives based on neuroendocrine changes in rodent models, Neurodegener. Dis. 6 (2009) 154–164.
[45] J. Sassone, C. Colciago, G. Cislaghi, V. Silani, A. Ciammola, Huntington's disease: the current state of research with peripheral tissues, Exp. Neurol. 219 (2009) 385–397.
[46] J.M. van der Burg, M. Bjorkqvist, P. Brundin, Beyond the brain: widespread pathology in Huntington's disease, Lancet Neurol. 8 (2009) 765–774.